ELSEVIER

Polymer Vol. 37 No. 5, pp. 745–754, 1996

0032-3861/96/$15.00+0.00

Phonons in 7_2 helical poly(4-methyl-1-pentene)

G. P. Bahuguna
Lucknow Christian Degree College, Lucknow, India

and Shantanu Rastogi, Poonam Tandon and V. D. Gupta*
Physics Department, Lucknow University, Lucknow 226 007, India
(Received 25 April 1995)

The normal modes and their dispersions for isotactic poly(4-methyl-1-pentene) have been obtained in the reduced zone scheme using Wilson's GF matrix method as modified by Higgs. The zone centre frequencies and Urey–Bradley potential field have been obtained by fitting the observed Fourier transform infra-red absorption bands. Some of the characteristic features of the dispersion curves are repulsion, exchange of character and Von Hove type singularities. The heat capacity obtained from the density-of-states agrees with the experimental data up to 305 K, at which glass transition sets in and the experimental curve exhibits a marked change in slope.

(Keywords: poly(4-methyl-1-pentene); phonon dispersion; density-of-states)

INTRODUCTION

Isotactic poly(4-methyl-1-pentene) (P4MP1) consists of a polymethylene chain with $-CH_2-CH-(CH_3)_2$ as side group on every second carbon atom along the chain (*Figure 1* shows one chemical repeat unit). Its exceptionally low density, transparency and high softening point make it a commercially important polymer[1]. Because of unusual loose packing, the density of the crystalline phase is less than that of the amorphous phase.

The simple polymethylene chain in the usual paraffins and polyethylene takes up a planar zig-zag configuration. The presence of side groups throws the chain in a helical form due to steric interference, the helicity depending on the nature of the side group. In the particular case of P4MP1, the side group $-CH_2-CH-(CH_3)_2$ gives it an approximate 7_2 helix. The deviation from this uniform 7_2 helix is small in comparison with poly(ethylene oxide), which also has a 7_2 helix but no side chain. Further, the crystal structure of P4MP1 has a statistical disorder with respect to the upward and downward sense of the isomorphous helix[2]. This knowledge is important for an understanding of the spectra and spectral features.

Recent publications[3–8] on phonon dispersion in a variety of conformational states of polymers have demonstrated its potential in the fuller interpretation of Raman and infra-red (i.r.) spectra in addition to the interpretation of heat capacity measurements. Gabbay and Stivala[9] have reported an i.r. study of P4MP1. This study is, however, incomplete and the assignments are based purely on qualitative considerations. In the present paper we report complete normal mode analysis, phonon dispersions and density-of-states for P4MP1. The density-of-states is used to calculate heat capacity which enables us to correlate microscopic behaviour with macroscopic properties. The heat capacity data compare well with the heat capacity measurements reported by Karasz *et al.*[10].

* To whom correspondence should be addressed

THEORY

X-ray studies show[2] that iso-P4MP1 has a tetragonal unit cell, space group $P\bar{4}b_2$, with $a = b = 18.70$ Å and c (along the fibre axis) $= 13.68$ Å. For the present analysis the structure (model I) proposed by Kusanagi *et al.*[2] has been used. The internal rotation angles are $\tau_1 = 165°$, $\tau_2 = -72°$, $\tau_3 = 40°$ and $\tau_4 = 50°$, where

$$\tau_1 = (C_\varepsilon^{-1}\text{–}C_\alpha^{-1}\text{–}C_\varepsilon\text{–}C_\alpha) \qquad \tau_2 = (C_\alpha^{-1}\text{–}C_\varepsilon\text{–}C_\alpha\text{–}C_\varepsilon^{+1})$$

$$\tau_3 = (H\text{–}C_\alpha\text{–}C_\beta\text{–}C_\gamma) \qquad \tau_4 = (C_\alpha\text{–}C_\beta\text{–}C_\gamma\text{–}H)$$

The bond lengths and bond angles used are: C–C = 1.54 Å, $\angle C\text{–}CH_2\text{–}C = 114°$ and all other bond angles are 109.5°.

Calculation of normal mode frequencies

The calculation of normal mode frequencies has been carried out according to Wilson's GF matrix method[11] as modified by Higgs[12] for an infinite chain. This method consists of writing the inverse kinetic energy matrix **G** and the potential energy matrix **F** in internal coordinates R. In the case of an infinite isolated helical polymer, there are an infinite number of internal coordinates which lead to **G** and **F** matrices of infinite order. Due to the screw symmetry of the polymer, a transformation similar to that given by Born and Von Karman can be performed which reduces the infinite problem to finite dimensions.

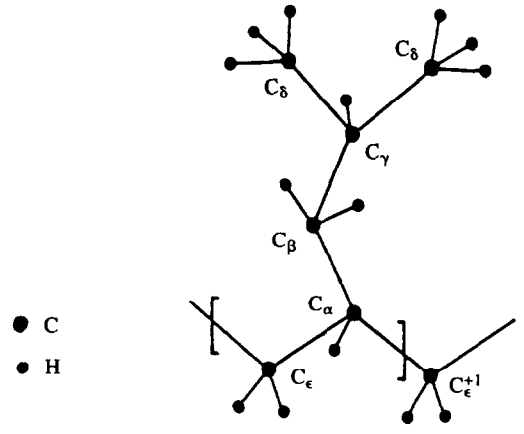

Figure 1 Chemical repeat unit of poly(4-methyl-1-pentene)

The transformation consists of defining a set of symmetry coordinates

$$S(\delta) = \sum_{s=-\infty}^{\infty} R^n \exp(is\delta)$$

where δ is the vibrational phase difference between the corresponding modes of the adjacent residue units.

The elements of the $\mathbf{G}(\delta)$ and $\mathbf{F}(\delta)$ matrices have the form

$$G_{ik}(\delta) = \sum_{s=-\infty}^{\infty} G_{ik}^s \exp(is\delta)$$

$$F_{ik}(\delta) = \sum_{s=-\infty}^{\infty} F_{ik}^s \exp(is\delta)$$

The vibrational secular equation which gives normal mode frequencies and their dispersion as a function of phase angles has the form

$$[\mathbf{G}(\delta)\mathbf{F}(\delta) - \lambda(\delta)I] = 0 \qquad 0 \leq \delta \leq \pi$$

The vibration frequencies $\nu(\delta)$ (in cm^{-1}) are related to eigenvalues $\lambda(\delta)$ by the following relation:

$$\lambda(\delta) = 4\pi^2 c^2 \nu^2(\delta)$$

For any given phase difference δ (other than 0 or π), the $\mathbf{G}(\delta)$ and $\mathbf{F}(\delta)$ matrices are complex. In order to avoid the difficulties involved in handling complex numbers, methods have been devised to transform the complex matrices into equivalent real matrices by constructing suitable linear combinations of coordinates. One method of transforming a complex matrix to its real matrix equivalent is through a similarity transformation. It can be shown that any complex matrix $\mathbf{H} = \mathbf{M} + i\mathbf{N}$ can be replaced by the real ones

$$\begin{vmatrix} \mathbf{M} & -\mathbf{N} \\ \mathbf{N} & \mathbf{M} \end{vmatrix}$$

In the present case, we can write $\mathbf{G}(\delta) = \mathbf{G}^R(\delta) + i\mathbf{G}^I(\delta)$ and $\mathbf{F}(\delta) = \mathbf{F}^R(\delta) + i\mathbf{F}^I(\delta)$, where $\mathbf{G}^R(\delta)$, $\mathbf{F}^R(\delta)$, $\mathbf{G}^I(\delta)$, $\mathbf{F}^I(\delta)$ are the real and imaginary parts of $\mathbf{G}(\delta)$ and $\mathbf{F}(\delta)$. The product $\mathbf{H}(\delta) = \mathbf{G}(\delta)\mathbf{F}(\delta)$ becomes:

$$\mathbf{H}(\delta) = \begin{vmatrix} \mathbf{G}^R(\delta) & -\mathbf{G}^I(\delta) \\ \mathbf{G}^I(\delta) & \mathbf{G}^R(\delta) \end{vmatrix} \times \begin{vmatrix} \mathbf{F}^R(\delta) & -\mathbf{F}^I(\delta) \\ \mathbf{F}^I(\delta) & \mathbf{F}^R(\delta) \end{vmatrix}$$

$$= \begin{vmatrix} \mathbf{H}^R(\delta) & -\mathbf{H}^I(\delta) \\ \mathbf{H}^I(\delta) & \mathbf{H}^R(\delta) \end{vmatrix}$$

where

$$\mathbf{H}^R(\delta) = \mathbf{G}^R(\delta)\mathbf{F}^R(\delta) - \mathbf{G}^I(\delta)\mathbf{F}^I(\delta)$$

$$\mathbf{H}^I(\delta) = \mathbf{G}^R(\delta)\mathbf{F}^I(\delta) + \mathbf{G}^I(\delta)\mathbf{F}^R(\delta)$$

The matrix $\mathbf{H}(\delta)$ now has dimensions $2N \times 2N$. The eigenvalues, therefore, occur in pairs of equal values. The difficulty of dealing with complex numbers is thus avoided.

Force constant evaluation

The force constants have been obtained by least-squares fitting. In order to obtain the 'best fit' with the observed frequencies the following procedure is adopted. Initially approximate force constants are transferred from isotactic polypropylene[13] and other hydrocarbons having similar groups[14,15]. Thus, starting with the approximate $\mathbf{F}$ matrix $\mathbf{F}_o$ and the observed frequencies λ_{obs} (related through a constant), one can solve the secular matrix equation

$$\mathbf{G}\mathbf{F}_o\mathbf{L}_o = \mathbf{L}_o\lambda_o \qquad (1)$$

Let $\Delta\lambda i = \lambda i_{obs} - \lambda i_o$ in the above equation. It can be shown that in the first-order approximation

$$\Delta\lambda = \mathbf{J}\Delta\mathbf{F}$$

where $\mathbf{J}$ is computed from $\mathbf{L}_o$. We wish to compute the corrections to $\mathbf{F}_o$ so that the errors $\overline{\Delta\lambda}$ are minimized. We use the theory of least squares and calculate

$$\mathbf{J}'\mathbf{P}\overline{\Delta\lambda} = (\mathbf{J}'\mathbf{P}\mathbf{J})\overline{\Delta F}$$

where $\mathbf{P}$ is a weighting matrix and $\mathbf{J}'$ is the transpose of $\mathbf{J}$. The solution to this equation is obtained by inverting $(\mathbf{J}'\mathbf{P}\mathbf{J})$ to give

$$\overline{\Delta\mathbf{F}} = (\mathbf{J}'\mathbf{P}\mathbf{J})^{-1}\mathbf{J}'\mathbf{P}\overline{\Delta\lambda}$$

If the number of frequencies is greater than the number of $\mathbf{F}$ matrix elements, the matrix $\mathbf{J}'\mathbf{P}\mathbf{J}$ should be non-singular and we obtain the corrections ΔF which will minimize the sum of the weighted squares of the residuals. If the corrections ΔF are fairly large, the linear relation between force constant and frequency term in the matrix equation (1) breaks down. In such a situation, further refinement using higher-order terms in the Taylor's series expansion of $\Delta\lambda i$ is needed. This procedure has been developed by King and others[16].

The calculated frequencies at $\delta = 0$ and $\delta = 0.57\pi$ (helix angle $= 2 \times 2\pi/7$) are matched with observed i.r. frequencies. The Fourier transform infra-red (*FT* i.r.) spectrum (*Figures 2* and *3*) of P4MP1 has been recorded in the 4000–200 cm^{-1} frequency range in CsI on a Perkin–Elmer 1800 spectrophotometer, which was purged with dry nitrogen gas before recording the spectrum. Since the optically active modes correspond to phase values $\delta = 0$ and $\delta = 0.57\pi$, a reasonably good

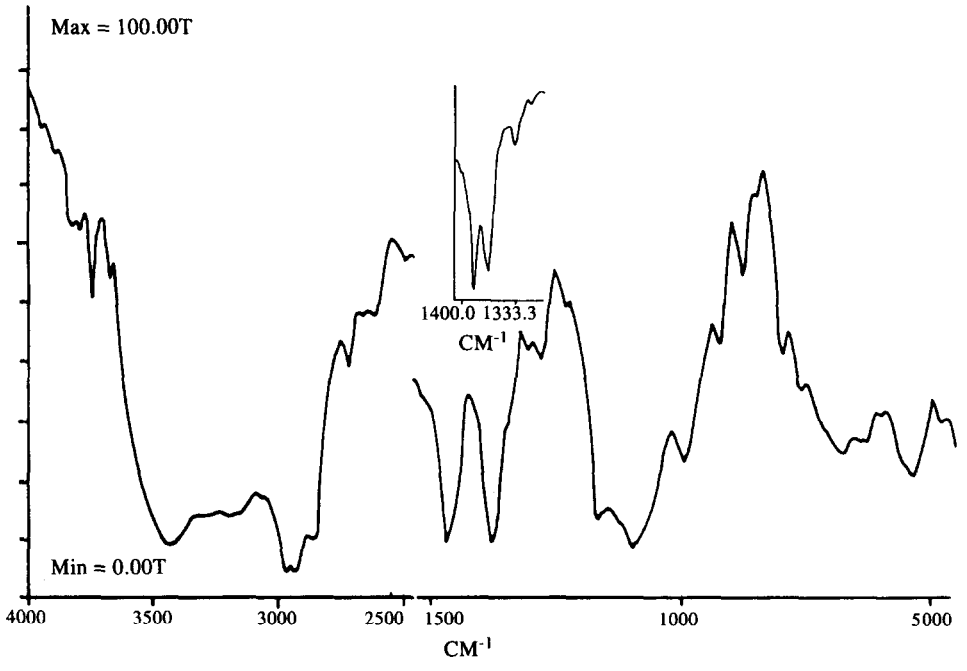

Figure 2 *FT*i.r. spectra of P4MP1 (4000–500 cm^{-1}). The *gem*-methyl group doublet is better resolved in inset

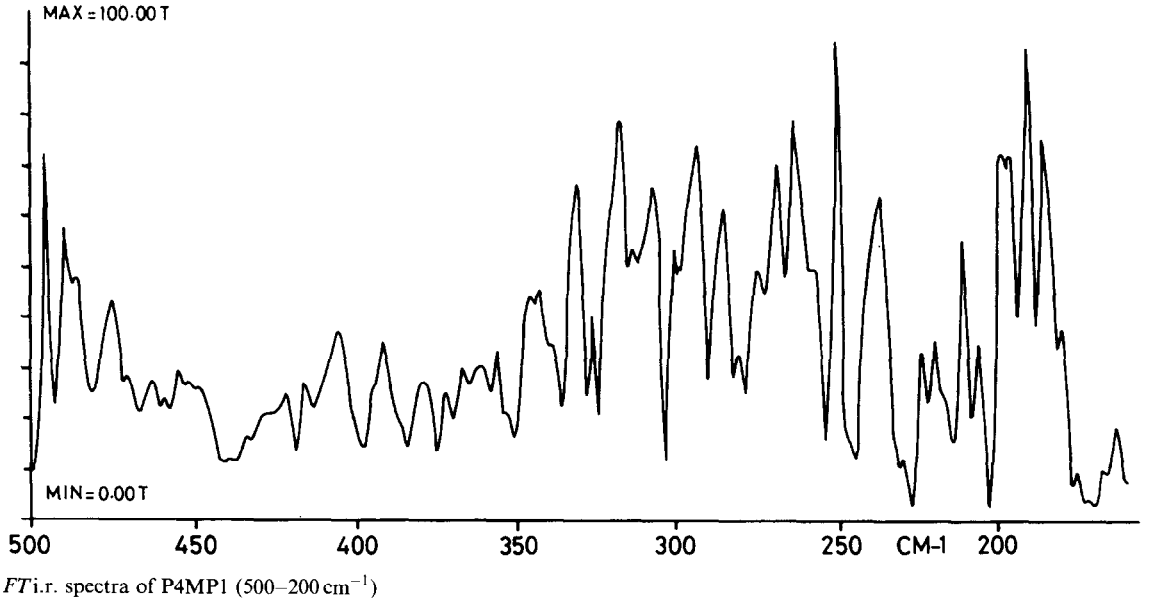

Figure 3 *FT*i.r. spectra of P4MP1 (500–200 cm^{-1})

matching is automatically obtained at $\delta = 0.57\pi$ by matching the observed frequencies at $\delta = 0$.

Calculation of specific heat

Dispersion curves, depicting the microscopic behaviour of the system, can be used to calculate macroscopic parameters of the system such as specific heat. The state density distribution function $g(\nu)$, giving the number of energy states in a unit interval of energy, for a one-dimensional system is given by

$$g(\nu) = \sum_j (\partial \nu_j / \partial \delta)^{-1}|_{\nu_j(\delta)=\nu}$$

The summation is over all branches (j) of normal modes. Considering the system as an assembly of harmonic oscillators, the distribution function $g(\nu)$ is equivalent to a partition function. The heat capacity at constant volume is then given by Debye's relation

$$C_v = \sum_j g(\nu_j) k N_A (h\nu_j/kT)^2 \frac{\exp(h\nu_j/kT)}{[\exp(h\nu_j/kT) - 1]^2} \quad (2)$$

with

$$\sum_j g(\nu_j) d\nu_j = 1$$

The constant volume heat capacity C_v, given by equation (2), is converted into constant pressure heat capacity C_p using the Nernst–Lindemann approximation

$$C_p - C_v = 3RA_o(C_p^2 T / C_v T_m^o)$$

Table 1 Force constants

Coordinate[a]	Value (mdyn Å^{-1})[b]	Coordinate[a]	Value (mdyn Å^{-1})[b]
1 $\nu(C_\delta-H)$	4.2000	15 $\phi(C_\varepsilon-C_\alpha-C_\varepsilon)$	0.4100 (0.175)
2 $\nu(C_\beta-H)$	4.1800	16 $\phi(C_\gamma-C_\delta-H)$	0.4150 (0.220)
3 $\nu(C_\varepsilon-H)$	4.1800	17 $\phi(H-C_\gamma-C_\delta)$	0.3820 (0.200)
4 ν $(C_\gamma-H)$	4.4100	18 $\phi(H-C_\beta-C)$	0.4220 (0.200)
5 $\nu(C_\alpha-H)$	4.4100	19 $\phi(H-C_\alpha-C_\varepsilon)$	0.3820 (0.200)
6 $\nu(C_\alpha-C_\beta)$	2.8500	20 $\phi(H-C_\varepsilon-C_\alpha)$	0.4220 (0.200)
7 $\nu(C_\gamma-C_\delta)$	2.5000	21 $\phi(H-C_\delta-H)$	0.4050 (0.295)
8 $\nu(C_\alpha-C_\varepsilon)$	3.1700	22 $\phi(H-C_\beta-H)$	0.4040 (0.295)
9 $\nu(C_\alpha-C_\varepsilon)$	2.8500	23 $\phi(H-C_\varepsilon-H)$	0.4040 (0.295)
10 $\phi(C_\delta-C_\gamma-C_\beta)$	0.4200 (0.175)	24 $\tau(C_\alpha-C_\beta)$	0.0250
11 $\phi(C_\alpha-C_\beta-C_\gamma)$	0.4200 (0.175)	25 $\tau(C_\gamma-C_\delta)$	0.0100
12 $\phi(C_\varepsilon-C_\alpha-C_\beta)$	0.4200 (0.175)	26 $\tau(C_\beta-C_\gamma)$	0.0175
13 $\phi(C_\delta-C_\gamma-C_\delta)$	0.4100 (0.175)	27 $\tau(C_\alpha-C_\varepsilon)$	0.0250
14 $\phi(C_\alpha-C_\varepsilon-C_\alpha)$	0.3800 (0.170)		
$\phi(H-C_\delta-C_\gamma) - \phi(H'-C'_\delta-C_\gamma)$ off-diagonal interactions:			
	0.0033}[c]		
	0.0067}[c]		
	0.0083}[c]		

[a] ν, ϕ and τ denote stretch, angle bend and torsion, respectively
[b] The values in parentheses are the corresponding non-bonded force constants
[c] Corresponding to the three positions of H and H′ in *gem*-dimethyl group

where A_0 is a constant and T_m° is the estimated equilibrium melting temperature. For P4MP1, $A_0 = 0.001 \times 10^{-3}$ K mol J^{-1} and $T_m^\circ = 522$ K.

RESULTS AND DISCUSSION

P4MP1 with 18 atoms in its repeat unit gives rise to 54 dispersion curves. The frequencies of vibrations were calculated at phase difference values from 0 to π at intervals of 0.05 π. The calculated frequencies at $\delta = 0$, ψ and 2ψ are optically active, where $\psi = 0.57\,\pi$. The force constants which give best fit to the observed *FT*i.r. spectra are given in *Table 1*.

Backbone modes (bb), side-chain modes (sc) and modes involving coupling of backbone and side-chain modes (bs) are presented in *Tables 2* to *4* at both the zone centre and helix angle, $\delta = 0.57\,\pi$. The potential energy distribution (PED) and the matched observed frequencies are shown alongside the calculated frequencies. The dispersions are plotted only for modes below 1350 cm^{-1} (*Figures 4a* and *5a*), because for frequencies above this the modes show no dispersion. The lower two dispersion curves correspond to the four acoustic modes: two at $\delta = 0$ to translation and rotation along the chain axis, and the other two at $\delta = 0.57\,\pi$ to transverse acoustic modes.

Side-chain modes

The dominant feature of the side chain of P4MP1 is a *gem* dimethyl group. Four calculated modes at 1472, 1471, 1470 and 1469 cm^{-1} are assigned to asymmetric degenerate deformation modes of CH_3. A band at 1469 cm^{-1} in the observed *FT*i.r. corresponds to these modes.

The observed frequencies at 1384 and 1368 cm^{-1} (inset of *Figure 2*) are identified as a symmetrical CH_3 bending doublet, a characteristic feature indicating the presence of two methyl groups attached to the same carbon atom. These modes calculated at 1394 and 1370 cm^{-1} show no dispersion. Similar doublets are reported for polyisobutene (1388 and 1362 cm^{-1})[17], poly(L-leucine) (1382 and 1364 cm^{-1})[18] and poly(L-valine) (1390 and 1368 cm^{-1})[18].

The CH_2 scissoring modes in the main and side chains are calculated at 1455 and 1437 cm^{-1} respectively. These are conformationally independent and are matched to the observed frequencies 1456 and 1437 cm^{-1}. The side-chain CH_2 scissoring mode in poly(L-leucine)[18] at 1449 cm^{-1} supports this assignment. In this region Gabbay and Stivala[9] have reported frequencies at 1460 and 1439 cm^{-1} which are assigned respectively to CH_3 as-degenerate deformation and CH_2 scissoring modes.

The frequency at 1317 cm^{-1} has been assigned to side-chain C–C stretch and CH_2 wag. The frequency at 1007 cm^{-1} has a major contribution from the CH_3 rocking mode while a pure CH_3 rocking mode calculated at 909 cm^{-1} is matched to a frequency at 918 cm^{-1}, a strong band observed in *FT*i.r. This is in agreement with the assignment of Gabbay and Stivala[9].

Backbone modes

The backbone CH stretch, CH_2 stretch and CH_2 scissoring modes are calculated at 2927, 2899, 2851 and 1437 cm^{-1} respectively and match well with the observed frequencies. Being highly localized, these modes are non-dispersive. A zone centre mode calculated at 1338 cm^{-1} having contributions from CH_2 wag and C–C stretch, both belonging to bb, is matched with the observed frequency at 1337 cm^{-1}. This is in agreement with the assignment of 1333 cm^{-1} frequency reported by Gabbay and Stivala[9].

Table 2 Calculated and observed frequencies and potential energy distribution for side-chain modes

Frequency (cm^{-1})			Frequency (cm^{-1})	
Calc.	Obs.	%PED	Calc.	%PED
$\delta = 0$			$\delta = 0.57\pi$	
2962	2961	$\nu(C_\delta-H)(99)$	2962	$\nu(C_\delta-H)(99)$
2961		$\nu(C_\delta-H)(100)$	2961	$\nu(C_\delta-H)(100)$
2925	2926	$\nu(C_\gamma-H)(92)$	2925	$\nu(C_\gamma-H)(81)+\nu(C_\alpha-H)(17)$
2902		$\nu(C_\beta-H)(92)$	2902	$\nu(C_\beta-H)(92)$
2885	2882	$\nu(C_\delta-H)(100)$	2885	$\nu(C_\delta-H)(100)$
2885		$\nu(C_\delta-H)(100)$	2885	$\nu(C_\delta-H)(100)$
2885		$\nu(C_\delta-H)(99)$	2885	$\nu(C_\delta-H)(99)$
2884		$\nu(C_\delta-H)(100)$	2884	$\nu(C_\delta-H)(100)$
2852	2855	$\nu(C_\beta-H)(99)$	2852	$\nu(C_\beta-H)(97)$
1472	1469	$\phi(H-C_\delta H)(94)$	1472	$\phi(H-C_\delta-H)(94)$
1471		$\phi(H-C_\delta-H)(95)$	1471	$\phi(H-C_\delta-H)(95)$
1470		$\phi(H-C_\delta-H)(95)$	1470	$\phi(H-C_\delta-H)(95)$
1469		$\phi(H-C_\delta-H)(95)$	1469	$\phi(H-C_\delta-H)(95)$
1455	1456	$\phi(H-C_\beta-H)(78)+\phi(H-C_\beta-C)(17)$	1455	$\phi(H-C_\beta-H)(78)+\phi(H-C_\beta-C)(17)$
1394	1384	$\phi(C_\gamma-C_\delta-H)(47)+\phi(H-C_\delta-H)(46)$	1394	$\phi(C_\gamma-C_\delta-H)(47)+\phi(H-C_\delta-H)(46)$
1370	1368	$\phi(C_\gamma-C_\delta-H)(46)+\phi(H-C_\delta-H)(45)$	1370	$\phi(C_\gamma-C_\delta-H)(46)+\phi(H-C_\delta-H)(45)$
1029	1031	$\phi(H-C_\gamma-C_\delta)(32)+\phi(C_\gamma-C_\delta-H)(25)+\nu(C_\beta-C_\gamma)(17)$	1028	$\phi(H-C_\gamma-C_\delta)(32)+\phi(C_\gamma-C_\delta-H)(25)+\nu(C_\beta-C_\gamma)(17)$
1007		$\phi(C_\gamma-C_\delta-H)(51)+\phi(H-C_\gamma-C_\delta)(10)+\nu(C_\gamma-C_\delta)(10)$	1009	$\phi(C_\gamma-C_\delta-H)(48)+\nu(C_\gamma-C_\delta)(9)+\phi(H-C_\gamma-C_\delta)(9)$
986	1009	$\phi(C_\gamma-C_\delta-H)(30)+\nu(C_\gamma-C_\delta)(22)+$ $\phi(H-C_\gamma-C_\delta)(16)$	990	$\phi(C_\gamma-C_\delta-H)(19)+\nu(C_\gamma-C_\delta)(12)+\phi(H-C_\gamma-C_\delta)(11)+$ $\nu(C_\alpha-C_\beta)(11)+\nu(C_\alpha-C_\varepsilon)(10)$
872	874	$\phi(C_\gamma-C_\delta-H)(50)+\nu(C_\beta-C_\gamma)(24)+\nu(C_\gamma-C_\delta)(9)$	873	$\phi(C_\gamma-C_\delta-H)(53)+\nu(C_\beta-C_\gamma)(16)+\nu(C_\gamma-C_\delta)(16)$
858	846	$\phi(C_\gamma-C_\delta-H)(33)+\nu(C_\gamma-C_\delta)(32)+\nu(C_\alpha-C_\varepsilon)(9)$	864	$\phi(C_\gamma-C_\delta-H)(47)+\nu(C_\gamma-C_\delta)(23)+\nu(C_\beta-C_\gamma)(13)$
749	731	$\nu(C_\gamma-C_\delta)(55)+\phi(H-C_\beta-C)(14)+$ $\phi(C_\gamma-C_\delta-H)(9)$	751	$\nu(C_\gamma-C_\delta)(58)+\phi(H-C_\beta-C)(11)+\phi(C_\gamma-C_\delta-H)(10)+$ $\nu(C_\beta-C_\gamma)(9)$
54		$\tau(C_\alpha-C_\beta)(47)+\tau(C_\beta-C_\gamma)(38)$	58	$\tau(C_\beta-C_\gamma)(58)+\tau(C_\alpha-C_\beta)(15)+\phi(C_\varepsilon-C_\alpha-C_\beta)(12)$

Table 3 Calculated and observed frequencies and potential energy distribution for backbone modes

Frequency (cm^{-1})			Frequency (cm^{-1})	
Calc.	Obs.	%PED	Calc.	%PED
$\delta = 0$			$\delta = 0.57\pi$	
2927	2926	$\nu(C_\alpha-H)(90)$	2926	$\nu(C_\alpha-H)(80)+\nu(C_\gamma-H)(16)$
2899		$\nu(C_\varepsilon-H)(90)$	2900	$\nu(C_\varepsilon-H)(92)$
2851	2855	$\nu(C_\varepsilon-H)(99)$	2850	$\nu(C_\varepsilon-H)(97)$
1437	1437	$\phi(H-C_\varepsilon-H)(79)+\phi(H-C_\varepsilon-C_\alpha)(17)$	1438	$\phi(H-C_\varepsilon-H)(80)+\phi(H-C_\varepsilon-C_\alpha)(16)$

Note: Only dominant PEDs are given

Mixed modes and dispersion curves

Backbone–side chain junction modes, which are strongly coupled, show maximum dispersion (*Table 5*); for example, the mode calculated at 1148 cm^{-1} at $\delta = 0$ [PED:CH_2 bend (bb 43% and sc 23%) + CH bend (bb 22%)] disperses by 47 wave numbers and appears as 1101 cm^{-1} at $\delta = \pi$ [PED: CH_2 bend (sc 60%) + CH bend (bb 19%)]. Similarly, the 367 cm^{-1} band at $\delta = 0$ [PED: C–C–C bend (sc 41% and bb 21%) + CH bend (sc 17%)] disperses by 52 wavenumbers and has its PED changed at $\delta = \pi$ [C–C–C bend (sc 16% and bb 38%) + CH bend (sc 11% and bb 10%)]. The mode calculated at 139 cm^{-1} is another case of a strongly dispersed mode. Modes calculated at 1177, 785, 423, 332 and 102 cm^{-1} are some other mixed modes which disperse by about 20 to 30 wavenumbers.

Another dispersive mode at a lower frequency of 198 cm^{-1} is also a coupled mode and for this mode the methyl torsion contribution increases from 18% at $\delta = 0$ to 63% at $\delta = 0.39\pi$ where it has a frequency of 219 cm^{-1}. At this δ value it approaches very near the frequency of a pure methyl torsion mode (222 cm^{-1}) which shows no dispersion. Another methyl torsion mode which has an energy corresponding to 228 cm^{-1} at $\delta = 0$ disperses by 26 cm^{-1} on mixing with the (C_ε–C_α–C_β) bending mode. This mixing appears to be generally responsible for dispersion as it is further supported by the mode calculated at 1316 cm^{-1} ($\delta = 0$). It disperses by 30 cm^{-1}.

The mode at 889 cm^{-1} with CH_3 rock and backbone stretch contributions and a non-dispersive pure CH_3 rocking mode at 909 cm^{-1}, both of the same symmetry species, appear to cross. There being no mirror plane

Table 4 Calculated and observed frequencies and potential energy distribution for mixed modes

Frequency (cm^{-1})			Frequency (cm^{-1})		
Calc.	Obs.	%PED	Calc.	Obs.	%PED
$\delta = 0$			$\delta = 0.57\pi$		
1338	1337	$\phi(H-C_\varepsilon-C_\alpha)(43)+\nu(C_\alpha-C_\varepsilon)(37)+\phi(H-C_\alpha-C_\varepsilon)(12)$	1331		$\phi(H-C_\varepsilon-C_\alpha)(25)+\phi(H-C_\beta-C)(19)+\nu(C_\alpha-C_\varepsilon)(17)+\nu(C_\alpha-C_\beta)(12)+\phi(H-C_\alpha-C_\varepsilon)(11)$
1316	1317	$\phi(H-C_\beta-C)(42)+\nu(C_\beta-C_\gamma)(20)+\nu(C_\alpha-C_\beta)(14)$	1302	1297	$\phi(H-C_\varepsilon-C_\alpha)(30)+\phi(H-C_\beta-C)(24)+\nu(C_\alpha-C_\varepsilon)(15)+\nu(C_\beta-C_\gamma)(11)$
1216	1219	$\phi(H-C_\gamma-C_\delta)(38)+\phi(H-C_\beta-C)(20)+\nu(C_\gamma-C_\delta)(16)$	1224		$\phi(H-C_\alpha-C_\varepsilon)(24)+\phi(H-C_\varepsilon-C_\alpha)(21)+\phi(H-C_\gamma-C_\delta)(14)+\phi(H-C_\beta-C)(12)$
1209		$\phi(H-C_\gamma-C_\delta)(26)+\phi(H-C_\alpha-C_\varepsilon)(24)+\phi(H-C_\varepsilon-C_\alpha)(17)+\nu(C_\beta-C_\gamma)(9)$	1213		$\phi(H-C_\gamma-C_\delta)(42)+\nu(C_\gamma-C_\delta)(14)+\phi(H-C_\beta-C)(12)$
1177	1170	$\phi(H-C_\varepsilon-C_\alpha)(44)+\phi(H-C_\alpha-C_\varepsilon)(23)+\phi(H-C_\gamma-C_\delta)(14)$	1186		$\phi(H-C_\alpha-C_\varepsilon)(30)+\phi(H-C_\varepsilon-C_\alpha)(23)+\phi(H-C_\beta-C)(16)+\phi(H-C_\gamma-C_\delta)(16)$
1163		$\phi(H-C_\beta-C)(29)+\phi(H-C_\alpha-C_\varepsilon)(29)+\phi(H-C_\gamma-C_\delta)(24)$	1165		$\phi(H-C_\gamma-C_\delta)(31)+\phi(H-C_\beta-C)(21)+\phi(H-C_\alpha-C_\varepsilon)(19)+\phi(H-C_\varepsilon-C_\alpha)(12)$
1148	1150	$\phi(H-C_\varepsilon-C_\alpha)(43)+\phi(H-C_\beta-C)(23)+\phi(H-C_\alpha-C_\varepsilon)(22)$	1119	1130	$\phi(H-C_\varepsilon-C_\alpha)(34)+\phi(H-C_\beta-C)(28)+\phi(H-C_\alpha-C_\varepsilon)(24)$
1095	1100	$\phi(H-C_\beta-C)(49)+\phi(H-C_\alpha-C_\varepsilon)(24)+\phi(H-C_\varepsilon-C_\alpha)(10)$	1092		$\phi(H-C_\beta-C)(35)+\phi(H-C_\alpha-C_\varepsilon)(34)+\phi(H-C_\varepsilon-C_\alpha)(19)$
975	973	$\nu(C_\alpha-C_\beta)(33)+\nu(C_\alpha-C_\varepsilon)(16)+\phi(H-C_\varepsilon-C_\alpha)(15)+\phi(H-C_\alpha-C_\varepsilon)(12)$	979		$\phi(C_\gamma-C_\delta-H)(18)+\nu(C_\alpha-C_\varepsilon)(17)+\nu(C_\gamma-C_\delta)(14)+\phi(H-C_\gamma-C_\delta)(11)+\phi(H-C_\varepsilon-C_\alpha)(10)+\phi(H-C_\alpha-C_\varepsilon)(10)$
970	964	$\nu(C_\alpha-C_\varepsilon)(34)+\phi(C_\gamma-C_\delta-H)(20)+\phi(H-C_\alpha-C_\varepsilon)(11)+\nu(C_\gamma-C_\delta)(9)$	965		$\nu(C_\alpha-C_\varepsilon)(34)+\phi(C_\gamma-C_\delta-H)(18)+\nu(C_\alpha-C_\beta)(9)$
909	918	$\phi(C_\gamma-C_\delta-H)(90)$	909		$\phi(C_\gamma-C_\delta-H)(90)$
889		$\phi(C_\gamma-C_\delta-H)(36)+\nu(C_\alpha-C_\varepsilon)(18)+\phi(H-C_\beta-C)(12)$	900		$\nu(C_\alpha-C_\varepsilon)(24)+\nu(C_\alpha-C_\beta)(21)+\phi(C_\gamma-C_\delta-H)(18)+\phi(H-C_\varepsilon-C_\alpha)(12)+\phi(H-C_\beta-C)(10)$
806	815	$\phi(H-C_\beta-C)(41)+\phi(C_\gamma-C_\delta-H)(8)+\phi(H-C_\varepsilon-C_\alpha)(8)+\nu(C_\alpha-C_\beta)(8)+\nu(C_\alpha-C_\varepsilon)(8)$	814	815	$\phi(H-C_\beta-C)(46)+\nu(C_\gamma-C_\delta)(13)+\nu(C_\alpha-C_\varepsilon)(11)$
785	795	$\phi(H-C_\varepsilon-C_\alpha)(57)+\tau(C_\alpha-C_\varepsilon)(11)+\nu(C_\alpha-C_\varepsilon)(9)$	766	773	$\phi(H-C_\varepsilon-C_\alpha)(49)+\nu(C_\alpha-C_\varepsilon)(16)+\nu(C_\alpha-C_\beta)(9)+\tau(C_\alpha-C_\varepsilon)(9)$
423	419	$\phi(C_\varepsilon-C_\alpha-C_\beta)(29)+\phi(C_\alpha-C_\beta-C_\gamma)(15)+\phi(C_\alpha-C_\varepsilon-C_\alpha)(9)+\phi(C_\delta-C_\gamma-C_\beta)(8)$	432	433	$\phi(C_\varepsilon-C_\alpha-C_\beta)(27)+\phi(H-C_\alpha-C_\varepsilon)(19)+\tau(C_\alpha-C_\varepsilon)(9)+\phi(C_\delta-C_\gamma-C_\beta)(9)+\phi(C_\alpha-C_\varepsilon-C_\alpha)(8)$
367	369	$\phi(C_\delta-C_\gamma-C_\beta)(33)+\phi(C_\varepsilon-C_\alpha-C_\beta)(21)+\phi(H-C_\gamma-C_\delta)(17)+\phi(C_\alpha-C_\beta-C_\gamma)(8)$	387	383	$\phi(C_\varepsilon-C_\alpha-C_\varepsilon)(21)+\phi(C_\alpha-C_\beta-C_\gamma)(13)+\phi(C_\delta-C_\gamma-C_\beta)(12)+\phi(C_\varepsilon-C_\alpha-C_\beta)(8)$
332	336	$\phi(C_\delta-C_\gamma-C_\delta)(25)+\phi(C_\delta-C_\gamma-C_\beta)(18)+\phi(C_\varepsilon-C_\alpha-C_\beta)(18)$	354	350	$\phi(C_\delta-C_\gamma-C_\beta)(28)+\phi(H-C_\gamma-C_\delta)(18)+\phi(C_\delta-C_\gamma-C_\delta)(10)$
314	314	$\phi(C_\delta-C_\gamma-C_\beta)(28)+\phi(C_\delta-C_\gamma-C_\delta)(26)+\phi(C_\varepsilon-C_\alpha-C_\beta)(20)$	308	303	$\phi(C_\delta-C_\gamma-C_\delta)(38)+\phi(C_\delta-C_\gamma-C_\beta)(19)+\phi(C_\varepsilon-C_\alpha-C_\beta)(17)+\phi(C_\varepsilon-C_\alpha-C_\varepsilon)(8)$
265	267	$\phi(C_\varepsilon-C_\alpha-C_\varepsilon)(27)+\tau(C_\alpha-C_\varepsilon)(23)+\phi(C_\delta-C_\gamma-C_\beta)(15)+\phi(C_\delta-C_\gamma-C_\delta)(14)$	290	289	$\phi(C_\delta-C_\gamma-C_\beta)(22)+\phi(C_\varepsilon-C_\alpha-C_\beta)(15)+\phi(C_\alpha-C_\varepsilon-C_\alpha)(13)+\tau(C_\alpha-C_\varepsilon)(13)+\phi(C_\delta-C_\gamma-C_\delta)(10)$
228	228	$\tau(C_\gamma-C_\delta)(79)$	244	245	$\tau(C_\gamma-C_\delta)(37)+\phi(C_\delta-C_\gamma-C_\beta)(23)+\tau(C_\alpha-C_\varepsilon)(8)+\phi(C_\varepsilon-C_\alpha-C_\beta)(6)$
222	222	$\tau(C_\gamma-C_\delta)(99)$	223		$\tau(C_\gamma-C_\delta)(97)$
198	203	$\phi(C_\delta-C_\gamma-C_\beta)(18)+\tau(C_\gamma-C_\delta)(18)+\phi(H-C_\alpha-C_\varepsilon)(14)+\phi(C_\varepsilon-C_\alpha-C_\beta)(13)$	216	214	$\tau(C_\gamma-C_\delta)(44)+\phi(C_\delta-C_\gamma-C_\beta)(16)$
139		$\phi(C_\delta-C_\gamma-C_\beta)(24)+\phi(C_\alpha-C_\varepsilon-C_\alpha)(20)+\tau(C_\beta-C_\gamma)(16)+\tau(C_\alpha-C_\varepsilon)(10)$	186	187	$\tau(C_\gamma-C_\delta)(18)+\phi(C_\alpha-C_\beta-C_\gamma)(16)+\phi(C_\alpha-C_\varepsilon-C_\alpha)(10)+\phi(C_\varepsilon-C_\alpha-C_\beta)(9)+\tau(C_\alpha-C_\beta)(8)$
102		$\phi(C_\alpha-C_\beta-C_\gamma)(41)+\phi(C_\varepsilon-C_\alpha-C_\beta)(12)+\phi(H-C_\beta-C)(8)$	109		$\phi(C_\delta-C_\gamma-C_\beta)(20)+\phi(C_\alpha-C_\beta-C_\gamma)(16)+\tau(C_\beta-C_\gamma)(12)+\phi(C_\varepsilon-C_\alpha-C_\beta)(11)+\phi(C_\varepsilon-C_\alpha-C_\varepsilon)(10)$
41		$\tau(C_\alpha-C_\beta)(20)+\tau(C_\beta-C_\gamma)(18)+\phi(C_\alpha-C_\varepsilon-C_\alpha)(14)+\phi(C_\varepsilon-C_\alpha-C_\beta)(13)+\phi(H-C_\beta-C)(10)$	38		$\tau(C_\alpha-C_\beta)(30)+\phi(C_\varepsilon-C_\alpha-C_\beta)(20)+\tau(C_\alpha-C_\varepsilon)(15)$
0		—	26		$\tau(C_\alpha-C_\varepsilon)(47)+\tau(C_\alpha-C_\beta)(12)+\phi(C_\varepsilon-C_\alpha-C_\beta)(10)$
0		—	0		—

Note: Only dominant PEDs are given

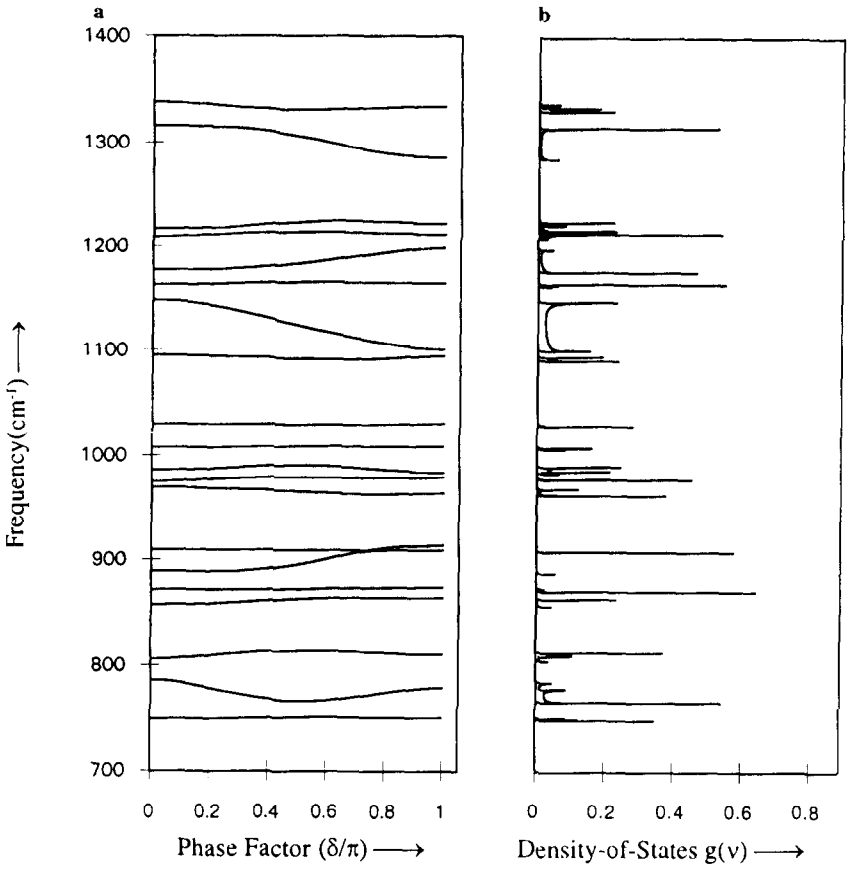

Figure 4 (a) Dispersion curves and (b) density-of-states curves of P4MP1 (1400–500 cm^{-1})

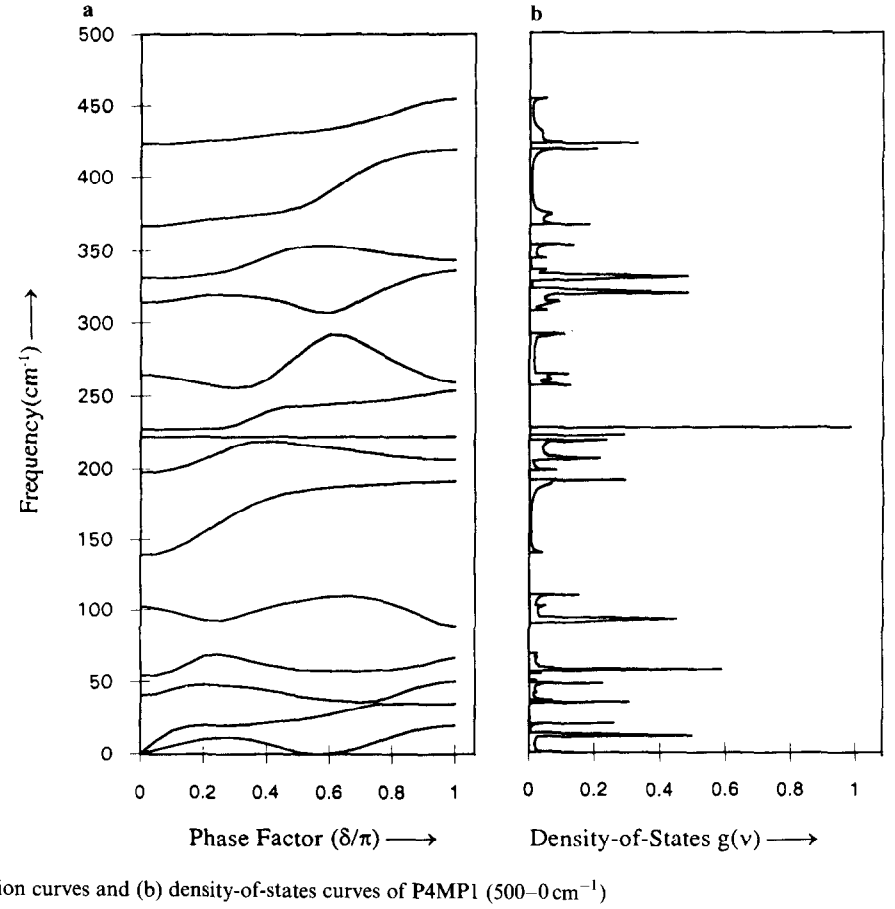

Figure 5 (a) Dispersion curves and (b) density-of-states curves of P4MP1 (500–0 cm^{-1})

Table 5 Characteristic features of dispersion curves

Frequency at $\delta = 0$ (cm^{-1})	Maximum dispersion frequency (cm^{-1}) (δ/π)	% PED
1338		$\phi(H-C_\varepsilon-C_\alpha)(43)+\nu(C_\alpha-C_\varepsilon)(37)+\phi(H-C_\alpha-C_\varepsilon)(12)$
	1331 (0.57)	$\phi(H-C_\varepsilon-C_\alpha)(25)+\phi(H-C_\beta-C)(19)+\nu(C_\alpha-C_\varepsilon)(17)+$ $\nu(C_\alpha-C_\beta)(12)+\phi(H-C_\alpha-C_\varepsilon)(11)$
1316		$\phi(H-C_\beta-C)(42)+\nu(C_\beta-C_\gamma)(20)+\nu(C_\alpha-C_\beta)(14)$
	1286 (1.0)	$\phi(H-C_\varepsilon-C_\alpha)(43)+\phi(H-C_\beta-C)(21)+\nu(C_\beta-C_\gamma)(12)+$ $\nu(C_\alpha-C_\varepsilon)(10)$
1216		$\phi(H-C_\gamma-C_\delta)(38)+\phi(H-C_\beta-C)(20)+\nu(C_\gamma-C_\delta)(16)$
	1224 (0.57)	$\phi(H-C_\alpha-C_\varepsilon)(24)+\phi(H-C_\varepsilon-C_\alpha)(21)+\phi(H-C_\gamma-C_\delta)(14)+$ $\phi(H-C_\beta-C)(12)$
1177		$\phi(H-C_\varepsilon-C_\alpha)(44)+\phi(H-C_\alpha-C_\varepsilon)(23)+\phi(H-C_\gamma-C_\delta)(14)$
	1199 (1.0)	$\phi(H-C_\gamma-C_\delta)(23)+\phi(H-C_\alpha-C_\varepsilon)(23)+\phi(H-C_\beta-C)(13)+$ $\phi(H-C_\varepsilon-C_\alpha)(11)+\nu(C_\alpha-C_\varepsilon)(10)$
1148		$\phi(H-C_\varepsilon-C_\alpha)(43)+\phi(H-C_\beta-C)(23)+\phi(H-C_\alpha-C_\varepsilon)(22)$
	1101 (1.0)	$\phi(H-C_\beta-C)(60)+\phi(H-C_\alpha-C_\varepsilon)(19)+\phi(H-C_\gamma-C_\delta)(9)$
806		$\phi(H-C_\beta-C)(41)+\phi(C_\gamma-C_\delta-H)(8)+\phi(H-C_\varepsilon-C_\alpha)(8)+$ $\nu(C_\alpha-C_\beta)(8)+\nu(C_\alpha-C_\varepsilon)(8)$
	814 (0.57)	$\phi(H-C_\beta-C)(46)+\nu(C_\gamma-C_\delta)(13)+\nu(C_\alpha-C_\varepsilon)(11)$
785		$\phi(H-C_\varepsilon-C_\alpha)(57)+\tau(C_\alpha-C_\varepsilon)(11)+\nu(C_\alpha-C_\varepsilon)(9)$
	766 (0.57)	$\phi(H-C_\varepsilon-C_\alpha)(49)+\nu(C_\alpha-C_\varepsilon)(16)+\nu(C_\alpha-C_\beta)(9)+\tau(C_\alpha-C_\varepsilon)(9)$
423		$\phi(C_\varepsilon-C_\alpha-C_\beta)(29)+\phi(C_\alpha-C_\beta-C_\gamma)(15)+\phi(C_\alpha-C_\varepsilon-C_\alpha)(9)+$ $\phi(C_\delta-C_\gamma-C_\beta)(8)$
	455 (1.0)	$\phi(C_\varepsilon-C_\alpha-C_\varepsilon)(34)+\phi(H-C_\alpha-C_\varepsilon)(18)+(C_\alpha-C_\varepsilon-C_\alpha)(15)+$ $\tau(C_\alpha-C_\varepsilon)(9)$
367		$\phi(C_\delta-C_\gamma-C_\beta)(33)+\phi(C_\varepsilon-C_\alpha-C_\beta)(21)+\phi(H-C_\gamma-C_\delta)(17)+$ $\phi(C_\alpha-C_\beta-C_\gamma)(8)$
	419 (1.0)	$\phi(C_\varepsilon-C_\alpha-C_\beta)(24)+\phi(C_\delta-C_\gamma-C_\beta)(16)+\phi(C_\alpha-C_\varepsilon-C_\alpha)(14)+$ $\phi(H-C_\gamma-C_\delta)(11)+\phi(H-C_\alpha-C_\varepsilon)(10)+\tau(C_\alpha-C_\varepsilon)(8)$
332		$\phi(C_\delta-C_\gamma-C_\delta)(25)+\phi(C_\delta-C_\gamma-C_\beta)(18)+\phi(C_\varepsilon-C_\alpha-C_\beta)(18)$
	354 (0.57)	$\phi(C_\delta-C_\gamma-C_\beta)(28)+\phi(H-C_\gamma-C_\delta)(18)+\phi(C_\delta-C_\gamma-C_\delta)(10)$
228		$\tau(C_\gamma-C_\delta)(79)$
	254 (1.0)	$\tau(C_\gamma-C_\delta)(34)+\phi(C_\varepsilon-C_\alpha-C_\beta)(31)$
198		$\phi(C_\delta-C_\gamma-C_\beta)(18)+\tau(C_\gamma-C_\delta)(18)+\phi(H-C_\alpha-C_\varepsilon)(14)+$ $\phi(C_\varepsilon-C_\alpha-C_\beta)(13)$
	216 (0.57)	$\tau(C_\gamma-C_\delta)(44)+\phi(C_\delta-C_\gamma-C_\beta)(16)$
139		$\phi(C_\delta-C_\gamma-C_\beta)(24)+\phi(C_\alpha-C_\varepsilon-C_\alpha)(20)+\tau(C_\beta-C_\gamma)(16)+$ $\tau(C_\alpha-C_\varepsilon)(10)$
	191 (1.0)	$\tau(C_\alpha-C_\varepsilon)(26)+\phi(C_\delta-C_\gamma-C_\beta)(24)+\phi(C_\alpha-C_\beta-C_\gamma)(20)+$ $\tau(C_\gamma-C_\delta)(9)$
102		$\phi(C_\alpha-C_\beta-C_\gamma)(41)+\phi(C_\varepsilon-C_\alpha-C_\beta)(12)+\phi(H-C_\beta-C)(8)$
	109 (0.57)	$\phi(C_\delta-C_\gamma-C_\beta)(20)+\phi(C_\alpha-C_\beta-C_\gamma)(16)+\tau(C_\beta-C_\gamma)(12)+$ $\phi(C_\varepsilon-C_\alpha-C_\beta)(11)+\phi(C_\varepsilon-C_\alpha-C_\varepsilon)(10)$
	88 (1.0)	$\tau(C_\alpha-C_\beta)(33)+\tau(C_\alpha-C_\varepsilon)(14)+\phi(C_\varepsilon-C_\alpha-C_\beta)(11)+$ $\phi(C_\delta-C_\gamma-C_\beta)(10)+\phi(H-C_\beta-C)(10)+\tau(C_\beta-C_\gamma)(10)$

Note: Only dominant PEDs are given

symmetry along the helix axis for P4MP1, the modes are not allowed to cross[17]. Further calculations at very close δ intervals (0.025π) confirm that it is not a case of crossing over. Instead, on coming close to each other the two modes mix, exchange character and get repelled.The two modes show repulsion near $\delta = 0.75\pi$ at which the higher one is repelled upwards and the lower one takes a constant value. Consequent to this the lower one becomes a pure CH_3 rocking mode while the upper one now has PED of the lower (*Table 6*, [I]). This is in agreement with the symmetry considerations.

The modes calculated at 265 cm^{-1} and 314 cm^{-1} (both at $\delta = 0$) undergo repulsion at $\delta = 0.64\pi$ and exchange their eigenvector energy contributions (*Table 6*, [II]).

For P4MP1 Gabbay and Stivala[9] have reported two bands at 844 (strong) and 810 cm^{-1} (medium) which are sensitive to both tacticity and crystallinity. In the present work these are observed at 846 and 815 cm^{-1} and

Table 6 Pairs of modes that repel and exchange character

Before exchange			After exchange		
Frequency (cm^{-1})	δ/π	% PED	Frequency (cm^{-1})	δ/π	% PED
[I]					
909	0.7	$\phi(C_\gamma-C_\delta-H)(83)$	911	0.8	$\nu(C_\alpha-C_\varepsilon)(29)+\phi(C_\gamma-C_\delta-H)(19)+\phi(H-C_\varepsilon-C_\alpha)(15)+\nu(C_\alpha-C_\beta)(14)$
907	0.7	$\nu(C_\alpha-C_\varepsilon)(26)+\phi(C_\gamma-C_\delta-H)(23)+\nu(C_\alpha-C_\beta)(16)+\phi(H-C_\varepsilon-C_\alpha)(14)$	909	0.8	$\phi(C_\gamma-C_\delta-H)(87)$
[II]					
308	0.57	$\phi(C_\delta-C_\gamma-C_\beta)(19)+\phi(C_\varepsilon-C_\alpha-C_\beta)(17)+\phi(C_\delta-C_\gamma-C_\delta)(38)$	316	0.70	$\phi(C_\delta-C_\gamma-C_\beta)(38)+\phi(C_\varepsilon-C_\alpha-C_\beta)(11)+\phi(C_\delta-C_\gamma-C_\delta)(11)$
290	0.57	$\phi(C_\delta-C_\gamma-C_\beta)(22)+\phi(C_\varepsilon-C_\alpha-C_\beta)(15)+\phi(C_\delta-C_\gamma-C_\delta)(10)$	287	0.70	$\phi(C_\delta-C_\gamma-C_\beta)(12)+\phi(C_\varepsilon-C_\alpha-C_\beta)(22)+\phi(C_\delta-C_\gamma-C_\delta)(31)$

Note: Only dominant PEDs are given

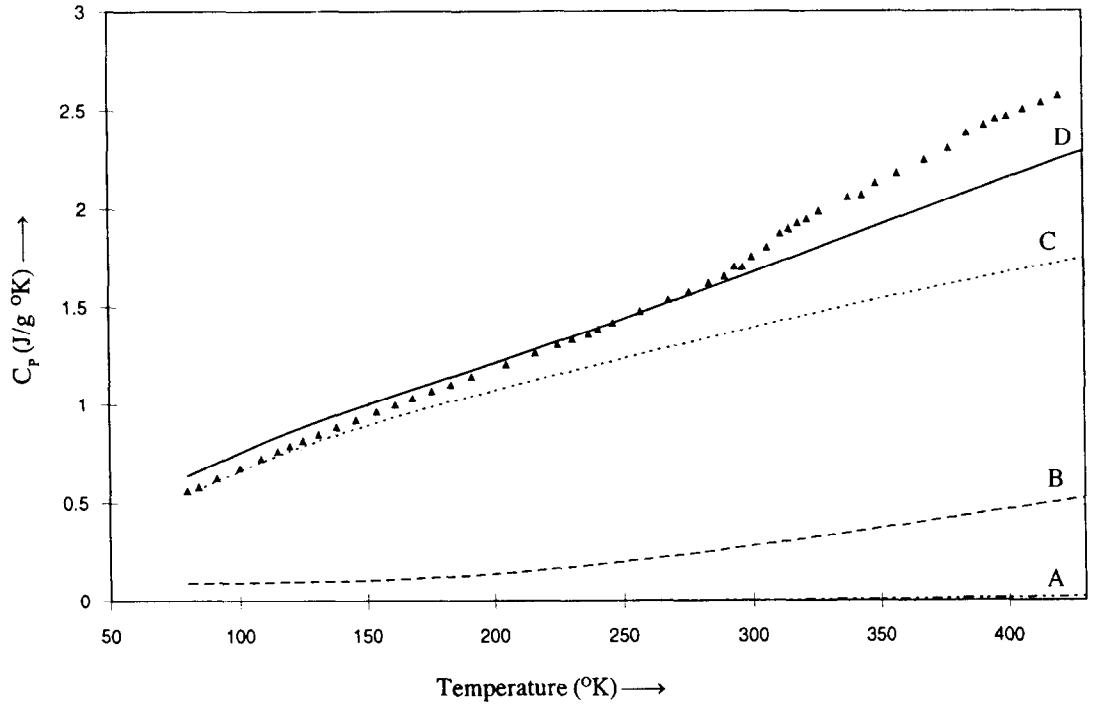

Figure 6 Heat capacity *versus* temperature plot of P4MP1 showing the contribution of backbone modes (A), side-chain modes (B) and mixed modes (C). (D) Total heat capacity. ▲, Experimental data

matched with the calculated values of 858 and 806 cm^{-1} respectively. Further, the bands at 833 (medium) and 717 cm^{-1} (strong) reported in the same work for the atactic P4MP1 do not appear in our observed or calculated spectra.

The good agreement between the experimental and calculated frequencies at $\delta = 0$ and $\delta = 0.57\pi$ shows that the profile of the dispersion curves is basically correct. The force field also reproduces well the observed frequencies down to 186 cm^{-1}. The above facts indicate the suitability of the model in the present investigation.

Density-of-states and heat capacity of P4MP1

Figures 4b and *5b* show the plots of density-of-states *versus* frequency as obtained from the dispersion curves. The peaks in the frequency distribution curves correspond to regions of high density-of-states (Von Hove type singularities)[19] which reproduce well the observed frequencies. Some of the observed peaks at 459, 374, 344, 324, and 208 cm^{-1} in the *FT*i.r. spectra, which could neither be assigned at $\delta = 0$ nor at $\delta = 0.57\pi$, can be respectively matched to the peaks at 454, 376, 345, 322 and 208 cm^{-1} in the frequency distribution curves.

From the frequency distribution curves, the heat capacity of P4MP1 has been calculated from 80 to 420 K. The contributions to the heat capacity are calculated separately for the side chain, backbone and mixed modes. These contributions are plotted in *Figure 6*. It is clear that the major contribution comes from the mixed modes. The sum of these three contributions gives the total heat capacity. The results show that the heat capacity is sensitive to the conformation of the chain, especially in the low frequency region. Our calculations of the heat capacity data are in good agreement with the experimental data of Karasz *et al.*[10]. The calculated data

also agree well with the data of the ATHAS Data Bank Update (1990)[20]. However, deviation is seen above 305 K, which is the glass transition temperature. Above this temperature the amorphous regions present in a polymer pass on to rubbery state in which the different segments along the chain backbone acquire energy to rotate around the covalent bonds due to increased thermal energy. These segmental motions are not taken into account in the normal mode calculations and cause the deviation. The glass transition temperature depends on the side group present, intermolecular cohesive forces and the chain geometry as these are sources of hindrance to the segmental mobility. In P4MP1 the bulky side group and regular geometry of the chain result in a higher glass transition temperature.

ACKNOWLEDGEMENTS

Financial assistance to G.P.B. from the University Grants Commission under the Teacher Fellowship Scheme and to V.D.G. from the Council of Scientific and Industrial Research under the Emeritus Scientist Scheme is gratefully acknowledged.

REFERENCES

1 Lopez, L. C., Wilkes, G. L., Stricklen, P. M. and White, S. A. *J. Macromol. Sci., Rev. Macromol. Chem. Phys.* 1992, **c32**(3&4), 301
2 Kusanagi, H., Takase, M., Chatani, Y. and Tadokoro, H. *J. Polym. Sci., Polym. Phys.* 1978, **16**, 131
3 Rastogi, S. and Gupta, V. D. *J. Macromol. Sci.–Phys.* 1994, **B33**(2), 129
4 Rastogi, S. and Gupta, V. D. *J. Macromol. Sci.–Phys.* 1995, **34**(1&2), 1
5 Burman, L., Tandon, P., Gupta, V. D., Rastogi, S., Srivastava, S. and Gupta, G. P. *J. Phys. Soc. Jpn.* 1995, **64**, 327
6 Gupta, A., Tandon, P., Gupta, V. D., Rastogi, S. and Gupta, G. P. *J. Phys. Soc. Jpn.* 1995, **64**, 315
7 Burman, L., Tandon, P., Gupta, V. D., Rastogi, S. and Srivastava, S. *Polym. J.* 1995, **27**, 481
8 Prasad, O., Tandon, P., Gupta, V. D. and Rastogi, S. *Polymer* 1995, **36**, 3739
9 Gabbay, S. M. and Stivala, S. S. *Polymer* 1976, **17**, 121
10 Karasz, F. E., Bair, H. E. and O'Reilly, J. M. *Polymer* 1967, **8**, 547
11 Wilson, E. B., Decuis, J. C. and Cross, P. C. 'Molecular Vibrations: The Theory of Infrared and Raman Vibrational Spectra', Dover Publications, New York, 1980
12 Higgs, P. W. *Proc. R. Soc. (London)* 1953, **A220**, 472
13 Snyder, R. G. and Schachtschneider, J. H. *Spectrochim. Acta* 1964, **20**, 853
14 Simanouti, T. *J. Chem. Phys.* 1949, **17**(8), 734
15 Simanouti, T. *J. Chem. Phys.* 1949, **17**(10) 848
16 King, W. T., Mills, I. M. and Crawford, B. L. *J. Chem. Phys.* 1957, **27**, 455
17 Bower, D. I. and Maddams, W. F. 'The Vibrational Spectroscopy of Polymers', Cambridge University Press, Cambridge, 1989, p. 154
18 Koenig, J. L. and Sutton, P. C. *Biopolymers* 1971, **10**, 89
19 Callaway, J. 'Quantum Theory of Solids', Academic Press, New York, London, 1974, p. 30
20 ATHAS Data Bank Update, University of Tennessee, Knoxville, USA 1990